FISEVIER

Contents lists available at ScienceDirect

Mechanical Systems and Signal Processing

journal homepage: www.elsevier.com/locate/ymssp



Full Length Article

Effective generation of shear horizontal waves from Lamb waves by meta-converters

Ze Liu^a, Shengbo Shan^{b,c,*}, Chuanzeng Zhang^{d,e}, Li Cheng^{a,f,*}

- ^a Department of Mechanical Engineering, The Hong Kong Polytechnic University, Kowloon, Hong Kong
- ^b Laboratory of Science and Technology on Integrated Logistics Support, College of Intelligent Science and Technology, National University of Defense Technology, Changsha 410073, PR China
- ^c School of Aerospace Engineering and Applied Mechanics, Tongji University, Shanghai 200092, PR China
- ^d Center for Mechanics Plus under Extreme Environments, Ningbo University, Ningbo 315211, PR China
- e Department of Civil Engineering, University of Siegen, Siegen D-57076, Germany
- ^f The Hong Kong Branch of National Rail Transit Electrification and Automation Engineering Technology Research Center, The Hong Kong Polytechnic University, Kowloon, Hong Kong

ARTICLE INFO

Keywords: Guided waves Shear horizontal (SH) waves Mode conversion Metamaterials Topology optimization Structural health monitoring (SHM)

ABSTRACT

Shear horizontal (SH) waves in thin-walled structures exhibit many advantages that are conducive to structural health monitoring (SHM) applications. However, their effective excitation is challenging in practice due to the inefficiency of shear-type piezoelectric transducers or the installation inconvenience of electromagnetic transducers. In this study, embracing the concept of metamaterials, we propose an SH wave generation scheme based on the mode conversion from Lamb waves activated by piezoelectric transducers. To this end, a metamaterial-mediated converter (referred to as a meta-converter), mounted on the surface of a host structure, is designed to achieve high-efficiency energy conversion from Lamb waves to SH waves. Targeting different Lamb wave modes in specific frequency bands, a topology optimization approach is developed to design the three-dimensional (3D) architecture of the meta-converters. The efficiency of the conversion is further evaluated in terms of the magnitude of the converted SH waves with respect to the incident Lamb waves. Analyses of band structures and mode shapes elucidate the mechanisms of the mode conversion within the targeted frequency band. Time-domain responses are analyzed to verify the efficient generation of SH waves, which are further illustrated by the visualizations of wave fields and wavenumber-frequency Fourier transform spectra. The robustness of the designed meta-converters is evaluated by examining piezoelectric transducers of different sizes. Finally, representative meta-converters are 3D-printed using the selective laser melting technique and tested for validation. The proposed method offers an alternative and feasible route for SH wave generation and paves a novel way for further SH-wave-based SHM applications.

1. Introduction

Shear horizontal (SH) waves are characterized by their in-plane polarization of particle motion that is perpendicular to the direction of wave propagation [1]. They exhibit appealing features for structural health monitoring (SHM) applications in thin-walled

E-mail addresses: shanshengbo25@nudt.edu.cn (S. Shan), li.cheng@polyu.edu.hk (L. Cheng).

Corresponding authors.

structures like the non-dispersion of SH0 waves [1,2], minimal mode conversion at cracks alongside simplified signal configuration [3,4], and no energy leakage to surrounding liquid media [5,6]. Moreover, SH waves can naturally satisfy the phase matching condition, thereby enabling the generation of cumulative third harmonic waves [7], which facilitates the detection of early-stage damage and defects [8]. In addition, the second harmonic SH waves have been shown to exhibit unique features, based on which SH-wave-based SHM has been developed to achieve highly sensitive detection of cracks, while preventing the interference from typical adverse factors in the measurement system, such as the nonlinearity from adhesive bonding layers [9].

The effective generation of SH waves is a crucial prerequisite for their SHM applications. Existing methods mainly rely on two types of transducers: electromagnetic acoustic transducers (EMATs) and shear-type PZT (Pb(ZrTi)) transducers. EMATs can be further broadly categorized into Lorentz-force-based types (e.g., periodic permanent magnet (PPM) EMAT) and magnetostriction-based types (e.g., magnetostrictive transducers (MsTs)). As a non-contact technique, the working principle of the PPM EMATs relies on the generation of a Lorentz force when a dynamic current flows through a static magnetic field. The resultant force is applied to the surface of a conductive structure to excite SH waves [10]. In contrast, MsTs operate based on the principle of shear deformation of a magnetostrictive patch, which can be surface-bonded on a structure and driven by a dynamic magnetic field produced by an AC-current coil in conjunction with a permanent magnet [11]. The efficacy of both PPM EMATs and MsTs for SH wave generation has been demonstrated in the open literature [8,12-15]. In particular, Seung et al. [16] designed an EMAT based on the Lorentz force to achieve omnidirectional SH wave excitation by employing a pair of ring-type permanent magnets. The omni-directivity of the EMAT for both SH wave generation and reception was validated experimentally. Wen et al. [4] developed a theoretical model of SH wave generation by MsTs based on the shear-lag model. Furthermore, the third harmonic SHO waves were employed to monitor early-stage material degradation, demonstrating their higher sensitivity in comparison with the commonly used second harmonic Lamb waves [8]. However, practical implementations of EMATs are challenging due to the use of coils and unwieldy magnets, which contradicts the SHM requirement for permanent installation of transducers. For the latter methods, typical shear-type PZT transducers, such as those using d_{15} [2,17,18], d_{36} [19,20], and d_{24} [21,22] modes, have also been explored for SH wave generation. For example, Belanger and Boivin [18] utilized the d_{15} mode of shear PZT transducers to generate omnidirectional SH waves. Miao et al. [21] acquired measurable SH waves as well using the d_{24} mode. Qiu et al. [23] developed a piezoelectric interdigital transducer for generating high-order SH waves. Compared with EMATs, PZT transducers are more in line with the online monitoring philosophy inherent in SHM. Unfortunately, PZTactivated SH waves are rather weak in intensity, which limits and even compromises their use in damage detection. These existing problems necessitate the development of novel and more effective methods for achieving efficient and stable SH wave generation.

It is well-known that Lamb waves can be readily excited in practice using typical d_{31} and d_{33} mode PZT transducers, whose effectiveness has been demonstrated in the guided-wave-based SHM applications [1]. One might logically wonder whether it is feasible to generate SH waves by means of converting Lamb waves into SH waves. While primary forms of mode conversions are difficult, the newly emerging concept of metamaterials, a kind of artificially architectured materials/structures, can potentially open new avenues to complete this task. In fact, existing works on metamaterials have shown their great promise in realizing various exotic wave manipulation phenomena, such as wave filtering [24], wave steering [25], mode conversion [26,27], cloaking [28], noise absorption [29], etc. Relevantly, only a limited number of studies have investigated the mode conversion from other types of elastic waves to SH waves [30-32]. For example, Kweun et al. [31] proposed specific resonance and coupling conditions for realizing maximum mode conversion from longitudinal waves into SH waves by using porous elastic metamaterials, thus offering theoretical guidance for efficient mode conversion at a fundamental level. To make the technique more applicable to SHM, Tian et al. [32] developed a nonperforated metamaterial converter, which is mounted on the surface of the structure to be inspected. In the targeted frequency band, only SH waves can pass while Lamb waves are filtered or converted, making SH waves dominant in the transmitted waves. However, from a practical perspective, the converted SH waves need to possess sufficiently high amplitudes to ensure effective wave-damage interaction, which is particularly critical for incipient damage monitoring. In addition, in order to keep the structure under inspection intact, any wave manipulation elements for SH wave generation should be surface-mounted instead of intrusively embedded. This necessitates the use of three-dimensional (3D) models to break the inherent structural symmetry, thus imposing additional complexity to the design process. Meanwhile, tone burst signals, commonly used in SHM, have a certain bandwidth, which requires the designed metamaterials to operate over a certain frequency band. These existing problems call for a systematic and holistic design approach to achieve efficient and band-targeted generation of SH waves.

Motivated by the aforementioned facts, we here propose an SH wave generation scheme based on the mode conversion from PZT-activated Lamb waves, with the help of tactically designed metamaterial-mediated converters (meta-converters) via topology optimization [33–36]. The meta-converters are consequently designed and fabricated to achieve high-efficiency Lamb waves to SH waves conversion. In a predefined operating frequency range (such as that of tone burst signals used in SHM [5,37,38]), typical scenarios involving incident Lamb waves of varying modes and frequencies are considered. The band structures and mode shapes are analyzed to elucidate the mechanisms of the mode conversion within the engineered frequency band. The effectiveness of the designed metaconverters is assessed through finite element (FE) simulations. Experiments using representative 3D-printed meta-converters are conducted for the final validation.

2. Topological designs of meta-converters

Given the high energy of Lamb waves activated by PZT transducers, meta-converters are to be designed and installed in the vicinity of the transducer to convert the PZT-activated Lamb waves into SH waves, as illustrated in Fig. 1. Fundamentally, the meta-converters need to be mounted on the surface of the host structure to ensure the structural integrity. To achieve efficient SH wave generation, this section presents metamaterial designs using a topology optimization method.

2.1. Topological optimization framework with 3D FE models

To maximize the SH wave generation, topology optimization of meta-converters is carried out, with the corresponding 3D model illustrated in Fig. 2(a). Specifically, Fig. 2(b) presents the schematic of the meta-converter to be topology-tailored. To facilitate practical implementation, a thin base layer with a thickness of h_{con} is added between the meta-converter to be designed and the host structure for ensuring the structural connectivity, as depicted in Fig. 2(b). The meta-converter on the base layer is discretized into $N \times N$ pixels in the x-y plane to enable the coupling between Lamb waves and SH waves. To reduce design variables, a 2D design domain is adopted in the x-y plane, as shown in Fig. 2(c). The design domain is characterized by a binary matrix, where "1" represents solid materials while "0" the vacuum. Note the height h_{meta} of the meta-converter, corresponding to the stretching length along the z-direction, plays a significant role in determining the properties of the meta-converter and is thus set as a design variable as well. This makes the current scheme a multi-scale topology optimization in terms of the micro-scale material distribution and the macro-scale geometry size.

Tone burst signals, which are commonly employed in SHM, contain a certain bandwidth within which the operating frequency of meta-converters should accommodate. In addition, based on the law of conservation of energy, maximizing SH waves inherently results in the minimization of Lamb waves. Therefore, we focus directly on SH waves in this study. Taking these concerns into consideration, the objective function and the constraints are formulated accordingly as:

maximizing:
$$\sum_{i}^{n} a_{i} Amp_{i}^{SH}(\Sigma)$$
 (1)

Subjected to:
$$\theta_{ij} = 0$$
 or $1 (i, j = 1, 2, ..., N)$, (2)

$$h_{meta} \leqslant h_{max}$$
, (3)

$$U(\Sigma) = U_1, \tag{4}$$

where Amp_i^{SH} represents the amplitude of SH waves at the i-th frequency component within the designed band, a_i is the corresponding weight, Σ denotes the material distribution inside the design domain, θ_{ij} represents the material selection of the i-j element, where 1 for solid materials and 0 for vacuum, and N is the dimension of the matrix. The height of the meta-converters, h_{meta} , expressed by a binary vector, should be smaller than a prescribed value h_{max} . Eq. (4) defines a maximum number U_1 of interconnected blocks within the design domain.

Genetic algorithm (GA) [39] is employed to generate new topologies during the optimization process. As a non-gradient optimization method, GA is mainly based on the principle of "survival of the fittest", where the performance of a structure is evaluated by its objective function. GA has been applied and proven effective in designing material configurations [34,40–42]. The GA used in this study operates as follows: A random population, containing *M* individuals, is first generated. Subsequently, the objective functions of all individuals are calculated based on FE results. Linear selection is performed based on fitness values to retain superior individuals. Uniform crossover and mutation are employed to produce offspring candidates. The single-elitism strategy is applied to preserve good genes, so as to accelerate the convergence of the optimization. So far, the next-generation individuals have been created. If the results have already converged or a prescribed number of iterations have been reached, output the best individual. Otherwise, return to the step of FE simulations for fitness evaluation and repeat the above procedure. The flow chart showing the GA-FE method based optimization procedure is given in Fig. 3.

The parameters of GA are set as follows: In light of the considerable computational cost associated with the 3D FE models, a population size of 24 is set as a compromise. In addition, the design domain is discretized into 16×16 pixels in the x-y plane. Linear selection, uniform crossover with a rate of 0.9, and uniform mutation with a rate of 0.03 are adopted. The maximum block number U_1 is set to one to facilitate fabrication. Additionally, the abuttal entropy processing [43] is involved to enhance topology quality. The

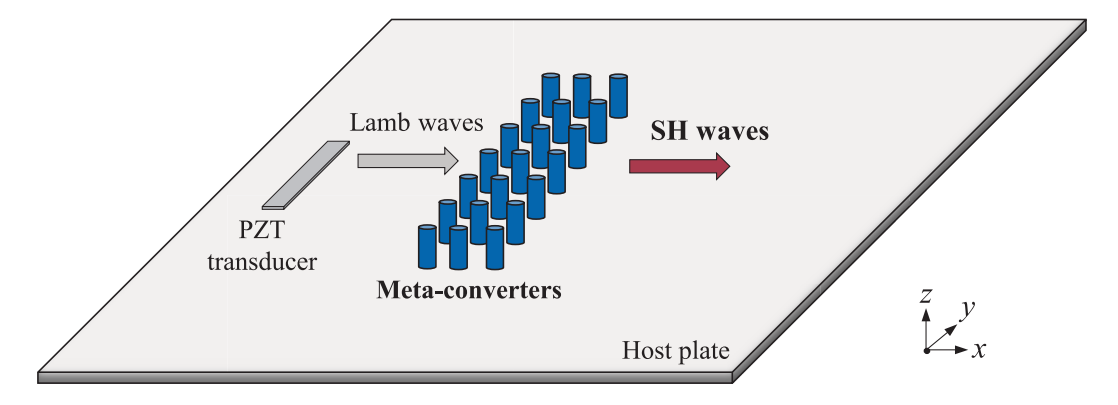


Fig. 1. Schematic of SH wave generation converted from PZT-activated Lamb waves with meta-converters.

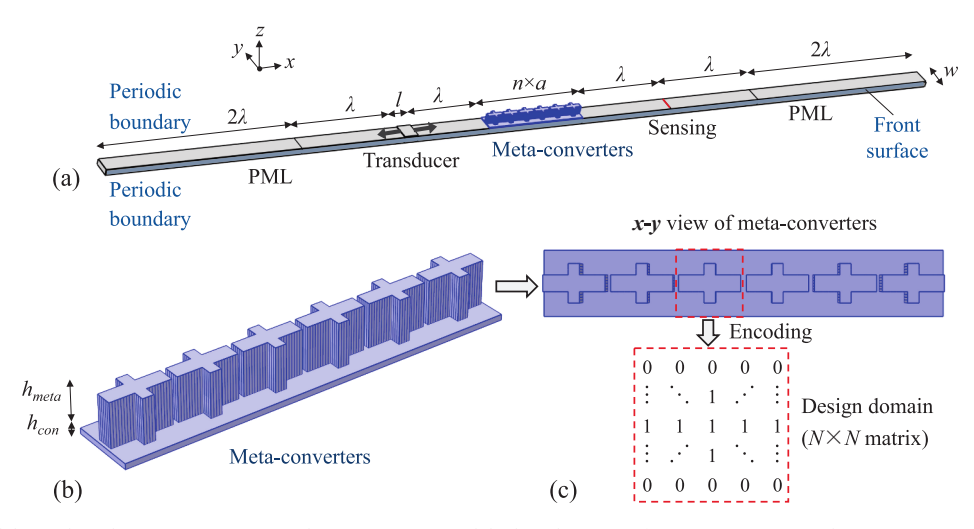


Fig. 2. FE models used in the optimization procedure: (a) entire model, (b) schematic of meta-converters, and (c) x-y (top) view of the meta-converter model, including the design domain.

optimization procedure is performed on a parallel computing workstation equipped with two Intel Xeon Scalable Gold 6248R CPU @3.0 GHz.

2.2. Optimized meta-converters

As a representative example, the central frequency is set to 200 kHz. Three discrete frequency points, namely 190, 200, and 210 kHz, are selected to represent the frequency band surrounding the central frequency. The corresponding assigned weights are $a_i = [1, 1.2, 1]$, respectively, to account for their relative contributions according to the frequency spectrum. To strike a balance between the computational cost and the performance, the meta-converter is constructed with six repeated unit cells (n = 6), each with dimensions of a = 4 mm and w = 4 mm. Similar cell numbers have been adopted in existing studies [27,30,31], with demonstrated effectiveness. Owing to its demonstrated reliable performance in elastic wave manipulation [44], steel is selected as the material for the meta-converters to facilitate fabrication via the selective laser melting 3D printing technique. Note that material selection is not a key concern in this study, and other materials, such as aluminum, could also be used to implement the proposed concept. The height of meta-converters, h_{meta} , is constrained to be less than 6 mm. The thickness of the base, h_{con} , is set to 0.3 mm, which is deemed an appropriate compromise between performance and fabrication requirements. An 8 mm-long PZT patch (l = 8 mm as featured in Fig. 2 (a)) is bonded on a 2 mm-thick aluminum plate. Note that the so-called length, width, and thickness in Fig. 2(a) refer to the dimensions in the x-, y-, and z-directions, respectively. The meta-converter and PZT transducer are attached to the host structure using 0.05 mm-

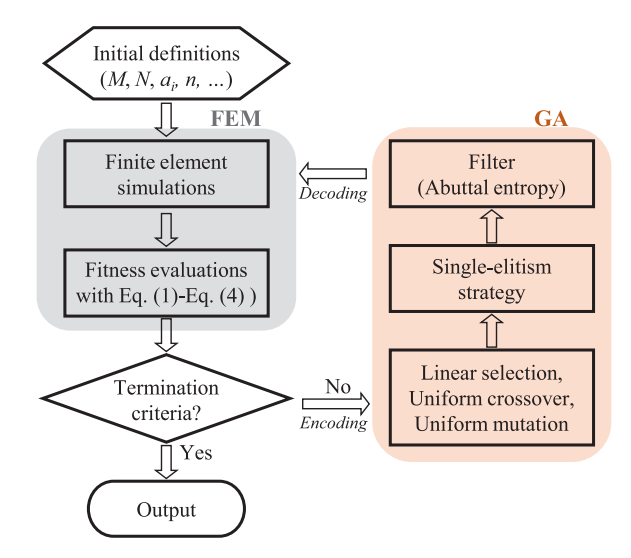


Fig. 3. Flow chart of GA-FEM (genetic algorithm-finite element method) based optimization procedure used in this study.

thick adhesive layers. The material parameters of different components are shown in Table 1. Note that for Lamb wave generations using PZT-5H, the d_{31} mode is dominant. Therefore, only the elastic constants associated with the d_{31} effect are considered, and the PZT material can be reasonably approximated as isotropic in the context of Lamb wave excitation.

Boundary loads with an amplitude of 50e5 N/m² along the *x*-direction are applied to the left and right surfaces of the PZT transducer for Lamb wave excitation, as shown in Fig. 2(a). The theoretical foundation for this treatment can be found in the literature [37,45], which used the shear lag model to simulate the mechanical behavior of PZT materials. Periodic boundary conditions are applied to the front and back surfaces of the model (the front surface is designated in Fig. 2(a)) in *y*-direction to guarantee the plane wave hypothesis. Perfectly matched layers (PMLs) are implemented at the left and right end regions of the model to minimize wave reflections. Quadratic serendipity is employed in FE discretization. Prism elements are used in the meta-converter domain to accommodate its complex geometry, while hexahedral elements are adopted for the remaining regions. The maximum size of the mapped meshes in FE models is set to 0.8 mm, ensuring at least 10 elements within the smallest wavelength under consideration. Along the thickness direction, the transducer, the host plate, and the adhesive layers are meshed into 7, 8, and 4 layers, respectively. The entire model consists of 106,438 elements, resulting in approximately 0.94 million degrees of freedom (when the design domain is fully filled with solid material). Frequency-domain analyses are conducted using COMSOL Multiphysics 5.2a, where the amplitudes of SH waves are captured in terms of the *y*-direction displacement in the transmitted wave field, as illustrated in Fig. 2(a). The entire optimization procedure takes approximately 65.6 h, involving roughly 100 iterations.

Three typical scenarios are considered, where the incident Lamb waves are set as (i) pure S (symmetric) mode Lamb waves, (ii) pure A (antisymmetric) mode Lamb waves, and (iii) combined S and A modes. By leveraging their inherent symmetry with respect to the plate thickness direction, single-mode Lamb waves can be excited through the symmetrical installation of PZT transducers at the upper and lower surfaces of the host plate, while the combinational waves can be generated with a single PZT transducer. Fig. 4 presents the optimized meta-converters corresponding to the above three cases, namely MC#1, MC#2, and MC#3, respectively. It is evident that all structures exhibit complex yet interconnected topologies, largely owing to the imposed geometry constraints and the added base layer, which collectively facilitate their eventual fabrication.

In order to evaluate the performance of the designed meta-converters, the amplitudes of the incident Lamb waves and the converted SH waves are extracted, which are normalized with respect to the maximum amplitude of the incident Lamb waves, respectively. Lamb waves are captured along the *x*-direction before the installation of meta-converters, whereas SH waves are captured along the *y*-direction after the deployment of the meta-converters. As evidenced by Fig. 5, high-amplitude SH waves are generated in all cases with meta-converters installed, while Lamb waves are significantly suppressed due to mode conversion, under different modes (S and A) and frequencies (190, 200, and 210 kHz). Notably, the amplitude ratio between the generated SH waves and the incident Lamb waves, which serves as an index to evaluate the performance of the meta-converters, can exceed one in some cases, as exemplified by the 210 kHz results in Fig. 5(a) and the 200 kHz results in Fig. 5(b). In addition, mode conversions between S and A mode Lamb waves are observed, as illustrated in Fig. 5. This exhibits the strong anisotropy feature of the designed meta-converters. The results demonstrate that effective mode conversions from Lamb waves to SH waves are achieved, thereby substantiating the efficacy of the designed meta-converters.

Moreover, the meta-converters are examined at other frequencies in the targeted frequency range, as exemplified by the case of MC#3. Figs. 6(a) and 6(b) present the amplitudes of Lamb waves and SH waves over the frequency range of 190–210 kHz, with a frequency interval of 1 kHz, without and with the meta-converter, respectively. All amplitudes are normalized with respect to the maximum incident Lamb wave amplitude. In addition to the prescribed frequency points [190, 200, 210] kHz used in the optimization, strong SH waves (with normalized amplitudes exceeding unity) are also observed in the remaining frequencies, as further visualized by the displacement wave fields at several intermediate frequencies, shown in Fig. 6(c). The results demonstrate the efficacy of the designed meta-converter over the frequency range.

2.3. Meta-converter-enabled mode coupling

The mechanism of the mode conversion from Lamb waves to SH waves roots in the formation of coupling modes that involve displacement components in all directions [31,46]. Guided by this principle, we define the design domain in the *x-y* plane during the meta-converter designs to intentionally disrupt the structural symmetry. Analyses of band structures and characteristic mode shapes for a representative meta-converter MC#3 are then conducted to further elucidate the mechanisms underpinning the generation of the mode conversion over the targeted frequency range.

For the calculation of band structures, the equation governing the elastic wave propagation in a heterogeneous elastic medium

Table 1Material parameters.

	Density (kg/m³)	Young's modulus (GPa)	Poisson's ratio
Aluminum	2700	70	0.33
Adhesive	1080	1.31	0.4
Steel	7980	180	0.26
PZT-5H	7650	62	0.32

For the PZT, the piezoelectric coefficients are $d_{31} = -210 \text{ pm/V}$ and $d_{33} = 472 \text{ pm/V}$, and the relative dielectric constants are $\varepsilon_{11} = 2270$ and $\varepsilon_{33} = 2130$, respectively, in which the subscripts 1 and 3 denote the x- and z-directions, respectively.

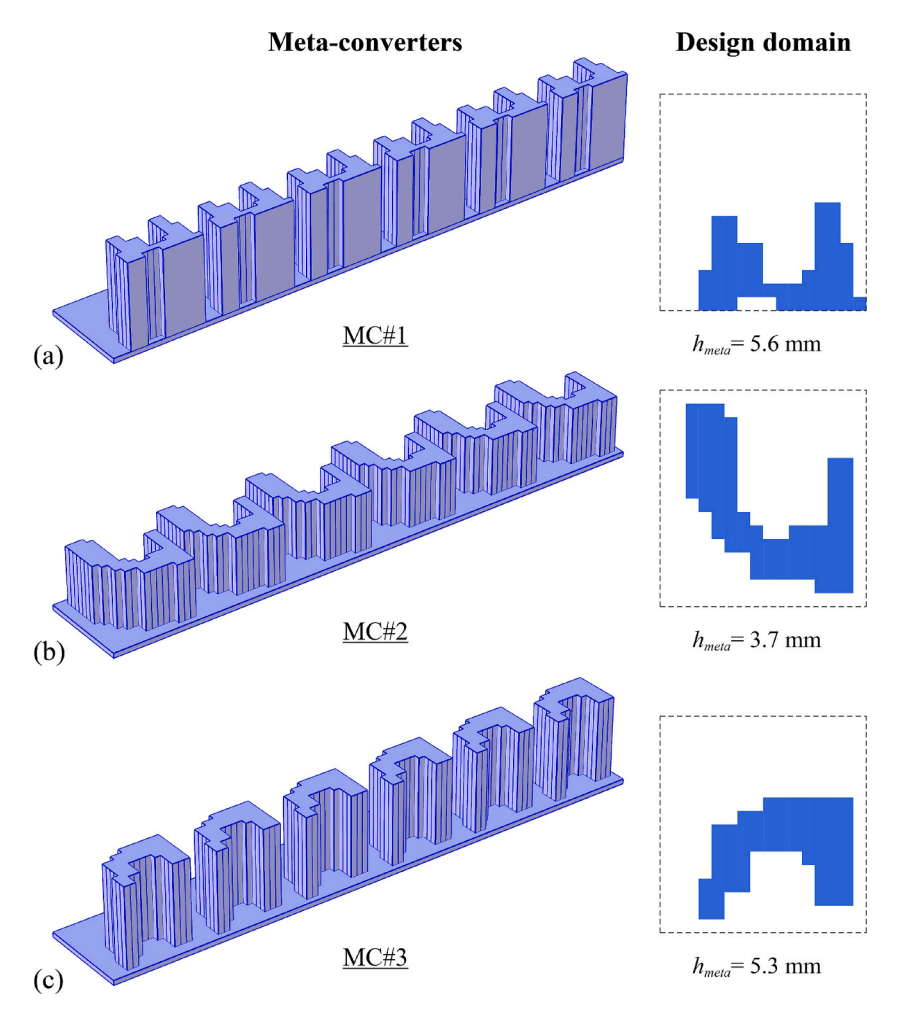


Fig. 4. Optimized meta-converters under incident waves of (a) pure S modes, (b) pure A modes, and (c) combined S and A modes.

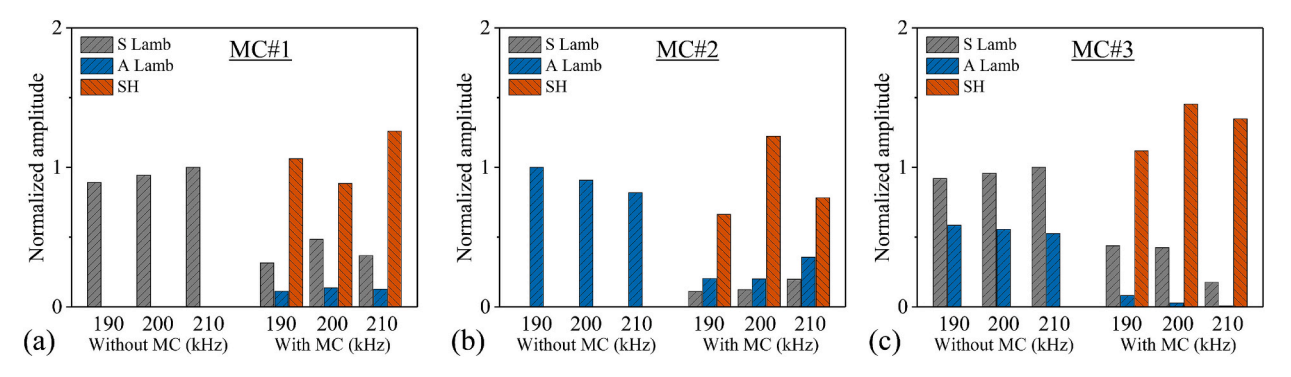


Fig. 5. Frequency-domain displacement amplitudes of different-mode wave components with/without the optimized meta-converters (a-c) MC#1-MC#3. All amplitudes are normalized with respect to the maximum amplitude of the incident Lamb waves, respectively.

writes [47]

$$\nabla\{[\lambda(\mathbf{r}) + 2\mu(\mathbf{r})](\nabla \cdot \mathbf{u}(\mathbf{r}, t))\} - \nabla \times [\mu(\mathbf{r})\nabla \times \mathbf{u}(\mathbf{r}, t)] + \rho(\mathbf{r})\ddot{\mathbf{u}}(\mathbf{r}, t) = 0,$$
(5)

where λ and μ denote the Lamé constants, ρ represents the mass density, \mathbf{r} is the position vector, \mathbf{u} denotes the particle displacement, and ∇ represents the gradient operator with respect to \mathbf{r} .

For periodic structures, the Bloch solution of the displacement vector can be expressed as [48]

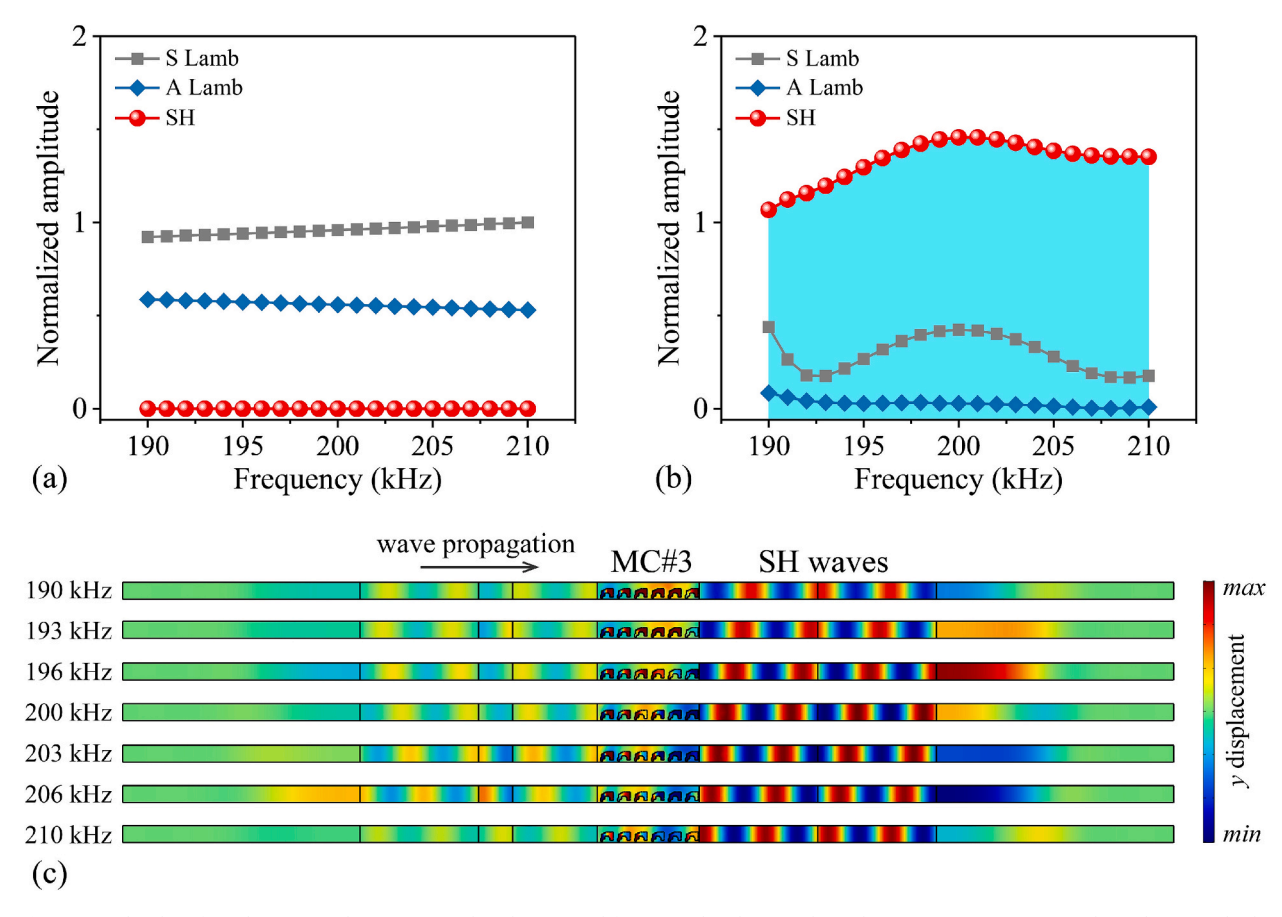


Fig. 6. Amplitudes of Lamb waves and SH waves within the targeted frequency band, (a) without the meta-converter MC#3, (b) with MC#3, both normalized with respect to the maximum incident Lamb wave amplitude, and (c) displacement fields of SH waves in the *x-y* plane at several intermediate frequencies.

$$\mathbf{u}(\mathbf{r},t) = \mathbf{u}_{\mathbf{k}}(\mathbf{r})e^{i(\mathbf{k}\cdot\mathbf{r}-\omega t)}. \tag{6}$$

where ${\bf k}$ is the wave vector, ${\bf u}_{\bf k}$ is a periodic function, and ω denotes the angular frequency. Furthermore, due to the Bloch periodic boundary condition, ${\bf u}$ takes the form of

$$\mathbf{u}(\mathbf{r} + \mathbf{a}, t) = \mathbf{u}(\mathbf{r}, t)e^{i(\mathbf{k} \cdot \mathbf{a})},\tag{7}$$

where a is the periodic constant vector.

FE method is adopted to solve the above problem. Substituting Eq. (6) into Eq. (5), the generalized eigenvalue problem can be expressed as

$$[\mathbf{K}(\mathbf{k}) - \omega^2 \mathbf{M}] \cdot \mathbf{U} = 0. \tag{8}$$

where **K** and **M** are the stiffness and mass matrices of the entire unit cell constructed from discrete elements, respectively, and **U** denotes the displacement matrix assembled from **u** of all elements. Equation (8) is then solved numerically using the commercial software COMSOL Multiphysics 5.2a, with the Bloch boundary condition in Eq. (7). To calculate the band structures, **k** is swept along the boundaries of the first irreducible Brillouin zone to obtain the corresponding frequencies ω [42,43].

An "eigenfrequency" study is performed in COMSOL Multiphysics 5.2a, based on the FE model of the unit cell shown in Fig. 7(a). Floquet (Bloch) periodic conditions (Eq. (7)) are applied to the lateral boundaries of the model (highlighted in blue in Fig. 7(a)). The wavevectors are swept along the Γ -X boundary within the first irreducible Brillouin zone, (0- π /a, 0, 0), to consider *x*-direction wave propagation. The mesh settings used here are identical to those employed in the previous model shown in Fig. 2(a).

Fig. 7(b) displays the band structures, while Fig. 7(c) presenting the extracted mode shapes at the considered frequency points [190, 200, 210] kHz. Hybrid mode shapes are observed, primarily exhibiting both bending (modes B_{12} and B_{22}) and torsional (modes B_{21} and B_{31}) deformation in the pillared regions. The mode shapes at the targeted frequencies confirm the presence of hybrid modes induced by the designed meta-converters. Compared with Lamb wave modes, whose displacements are confined in the x-z plane, the hybrid/coupled modes involve an additional y-direction component. This reveals the energy transfer path from Lamb waves to SH

waves. In addition, the energy, judged from the mode shapes, is distributed across different portions of the structure at different frequencies, suggesting the role played by multi-scattering phenomena in the multi-frequency function of the meta-converters. Furthermore, the band branches within the 190–210 kHz range appear to exhibit a consistent slope, as observed in the mode series B_{11} , B_{21} , and B_{31} (or B_{12} , B_{22} , and B_{32}) in Fig. 7(b). This signals the close group velocities within this frequency range, which additionally contribute to the synchronization feature of the meta-converters within this frequency band.

3. Numerical analyses

Time-domain analyses are then conducted to assess the performance of the designed meta-converters by taking MC#3 as a representative example. The simulation model in Fig. 2(a) is employed again, with the original PML settings disabled and their lengths extended to 4λ . 5-cycle tone burst with a central frequency of 200 kHz is used as excitation signal, whose total length is set to 9e-5 s with a time step of 2e-7 s. Fig. 8 presents the time-domain results, where the bare plate case serves as a reference to assess the intensity of the incident waves. In the bare plate, both S and A mode Lamb waves are excited, while SH waves are nearly zero. After deploying the meta-converter, high-amplitude SH waves are generated, as shown in Fig. 8(b), accompanied by a reduction in the intensity of Lamb waves due to the energy conversion (shown in Fig. 8(a)). Specifically, the generated SH waves attain an amplitude of 3.8e-8 m, which is comparable in magnitude to that of the incident Lamb waves. In addition, owing to the close group velocities within the frequency bands, as shown in Fig. 7(b), the distortion of SH waves is rather minimal and measurable wave packets are observed, which is conducive for their future applications in SHM.

Furthermore, using the 200 kHz frequency-domain data from Fig. 5(c), the amplitudes of the incident S, A mode Lamb waves, and that of the converted SH waves follow a ratio of 1:0.58:1.51. In contrast, the time-domain responses in Fig. 8 yield 1:0.58:0.6, indicating a discrepancy between the two analyses: stronger SH waves based on the frequency-domain data (Fig. 5(c)). This discrepancy is attributed to the different excitation forms. Specifically, in the frequency-domain analysis, the applied harmonic excitation is continuous over the entire time axis, resulting in a steady-state response at a single frequency. Conversely, the time-domain analysis employs a 5-cycle tone burst signal as the excitation, which exhibits a specific bandwidth centered at 200 kHz, thereby leading to limited mode conversion efficiency in the time-domain analysis, as the information is averaged across this frequency band. Nevertheless, both analyses explicitly demonstrate the effective generation of SH waves enabled by the designed meta-converter.

The displacement fields with/without the meta-converter are also extracted to visualize the conversion process in Fig. 9. Under PZT excitations, Lamb waves, including both S and A modes are clearly visible and propagate along the bare plate (upper-left sub-plot), with negligible SH wave components as demonstrated in the upper-right sub-plot. After deploying the meta-converter, SH waves clearly emerge in the transmitted wave field, as illustrated by the distinct wave packets in Fig. 9 (lower-right sub-plot).

Furthermore, the wavenumber-frequency Fast Fourier Transform (2D-FFT) is performed to classify different wave modes. A group of time-domain signals are extracted at the top surface of the plate with/without the meta-converters, respectively. To ensure sufficient resolution in the wavenumber domain, the sensing positions are selected with a total distance of 3.75λ and a space step of 0.1 mm. The results are then smoothened using linear interpolation. Fig. 10 presents the 2D-FFT results, expressed in terms of $20\log_{10}(|2\text{D-FFT}|/max(|2\text{D-FFT}|_{incident~S}))$, with $max(|2\text{D-FFT}|_{incident~S})$ being the maximum absolute value of the 2D-FFT results of the incident S mode Lamb waves. The dashed lines in Fig. 10 represent the theoretical dispersion curves. In the bare plate case, two spots are observed at 200 kHz in Fig. 10(a), which correspond to the S mode (with a theoretical wavenumber of 233 rad/m) and A mode (726 rad/m) Lamb waves, respectively. The SH waves displayed in Fig. 10(b) are found to be extremely weak. As a result of the meta-converter-enabled mode conversion, an SH wave-corresponding spot (403 rad/m) emerges, as shown in Fig. 10(d), which exhibits a comparable amplitude to that of the incident Lamb waves. This 2D-FFT analysis again demonstrates the successful conversion from Lamb waves achieved by the designed meta-converters.

In the original designs, an 8 mm-long PZT transducer is employed in the optimization process. To assess the influence of PZT

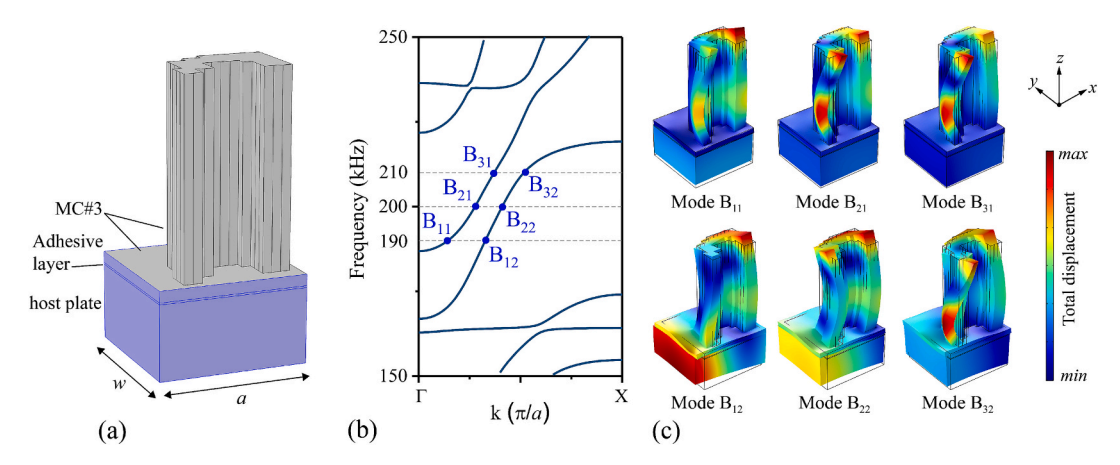


Fig. 7. (a) FE model, (b) band structures, and (c) representative mode shapes of the unit cells of the optimized meta-converter MC#3.

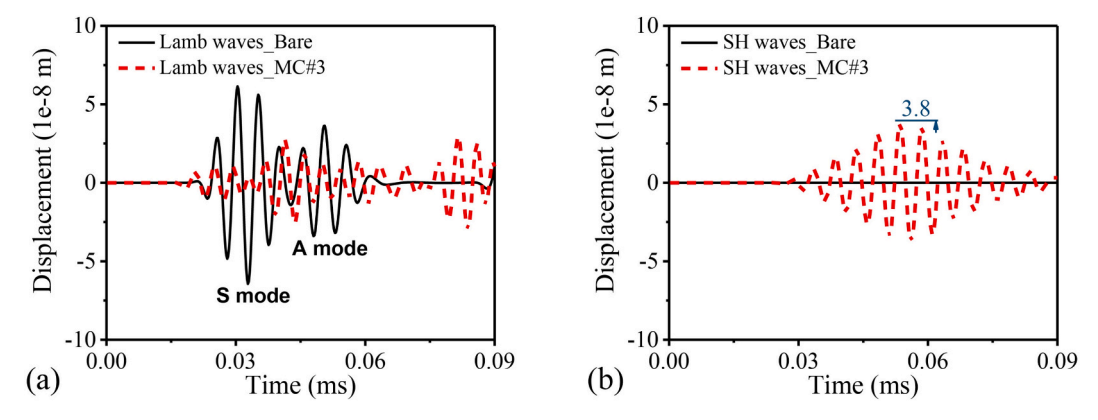


Fig. 8. Time-domain signals of (a) Lamb waves and (b) SH waves, with/without the optimized meta-converter MC#3.

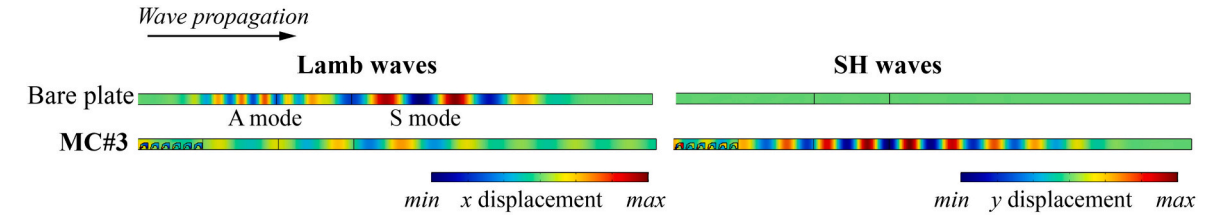


Fig. 9. Time-domain wave fields of the bare plate (upper row) and the case with the meta-converter MC#3 (lower row) in the x-y plane.

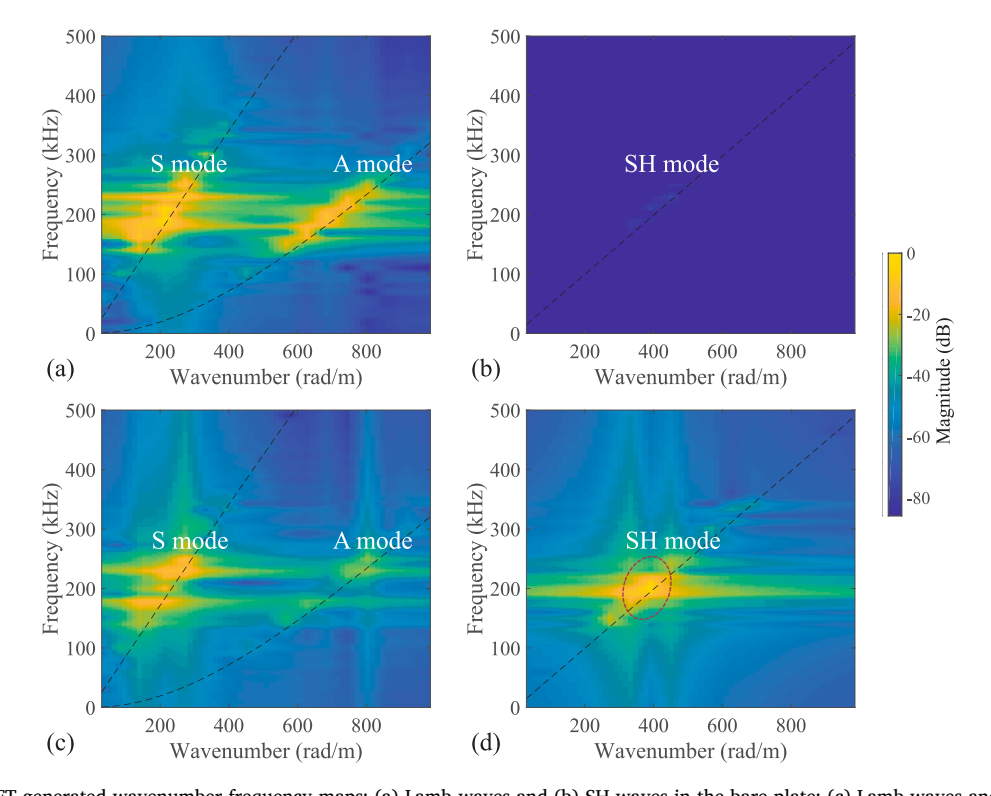


Fig. 10. 2D-FFT generated wavenumber-frequency maps: (a) Lamb waves and (b) SH waves in the bare plate; (c) Lamb waves and (d) SH waves with the meta-converter MC#3. Dashed lines represent the theoretical dispersion curves.

transducer size on the SH wave generation efficiency, we purposely vary the lengths of the PZT transducers from 4 mm to 22 mm. The corresponding amplitudes of incident Lamb waves and converted SH waves are extracted from time-domain signals and presented in Fig. 11. First and foremost, SH waves are generated in all cases, thereby confirming that the mode conversion function is an intrinsic property of the designed meta-converters, which can, in principle, be applied to other scenarios. Second, the curve of SH waves in Fig. 11 shows a trend with an initial increase followed by a gradual decline. This phenomenon can be attributed to the frequency tuning feature of the PZT transducers [45], which induces different amplitudes of incident S and A Lamb waves, as illustrated in Fig. 11, resulting in differences in the amplitudes of the generated SH waves. Specifically, according to the principle that maximum amplitude occurs when the PZT length equals to odd multiples of the half wavelength [37], the maximum S mode (approximately 27 mm in wavelength) amplitude is achieved when the PZT length is around 12–14 mm, while the maximum A mode (8.6 mm in wavelength) occurs at around 4–6 mm of PZT length. A more rigorous relationship between the PZT size and the excited Lamb wave amplitudes can be found in [37,45].

Furthermore, the performance of the designed meta-converter MC#3 is evaluated using a full-field 3D model. FE simulations are conducted using the 3D model shown in Fig. 12(a), with the model settings identical to those in Fig. 2(a). Nine unit cells (36 mm in total) are arranged along the y direction to match the size of the PZT actuator (30 mm in the same direction) for producing plane-like incident waves. Wave signals are captured at the point aligned with the center of the PZT in the y direction. This configuration helps mitigate the influence of the wavefront divergence, and the x- and y-direction displacements can still be used to represent Lamb waves and SH waves, as shown in Fig. 12(b) and 12(c), respectively. Specifically, Fig. 12(c) illustrates the wave field when the meta-converter is applied, clearly showing an SH wave packet. The corresponding time-domain signals in Fig. 12(e) confirm the generation of SH waves, alongside the reduced Lamb waves (Fig. 12(d)), with the deployment of the meta-converter.

4. Experimental validations

4.1. Experimental set-up and 3D-printing fabrication

Finally, experiments are carried out to validate the functionality of the designed meta-converters using MC#3 as an example. The test samples are fabricated using stainless steel 316 through the selective laser melting technique, which ensures high-resolution topologies, as illustrated in Fig. 13(b). Specifically, nine unit cells (36 mm in total) are installed in y-direction to ensure the structural periodicity, with numerically proven effectiveness shown in Fig. 12. 5-cycle tone burst signals with an amplitude of 150 V are applied on a PZT-5H transducer (8 mm \times 30 mm \times 0.3 mm) for Lamb wave generation. Due to the inherent difficulty in extracting SH waves in typical PZT-driven systems, MsTs are employed as the sensor. The MsT 4-fold coil has a periodicity distance of 15.5 mm to match the wavelength of the SH wave. Note that the MsTs is used here solely for SH wave measurements. All transducers and the meta-converter samples are surface-affixed on a 2024 T3 aluminum plate with dimensions of 700 mm \times 500 mm \times 2 mm. The MsT sensor is positioned 270 mm from the PZT transducer. Due to the finite size of the PZT actuator, the incident Lamb waves are not perfectly planar, especially in the far field. Therefore, the meta-converter should be positioned as close as possible to the PZT to minimize the wave divergence. Considering the practical installation constraints, the distance between the meta-converter and the actuator is set to 30 mm, which configuration is justified by the simulation results obtained using the full field model above (omitted for brevity).

The experimental set-up is shown in Fig. 13(a), with the measurement procedure operating as follows: 5-cycle tone burst signals with a central frequency of 200 kHz are input into the KEYSIGHT 33500B waveform generator. The generated signals are amplified to 150 V by the RITEC power amplifier to drive the PZT transducer. After the waves propagate across the meta-converter in the plate, the converted SH waves are received by the MsT sensor. Finally, the signals are sent to the National Instrument (NI) device equipped with a PXIe-5105 data acquisition module for further processing. Each measurement result is based on an average of 128 tests.

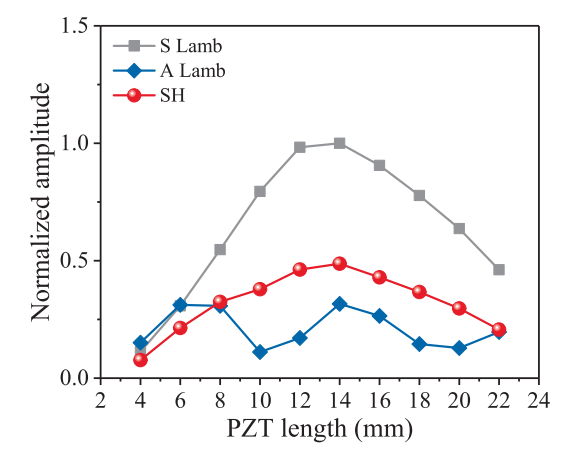


Fig. 11. Amplitudes of incident Lamb waves and converted SH waves, normalized with respect to the maximum incident Lamb wave amplitude, versus the length of PZT transducers with the meta-converter MC#3.

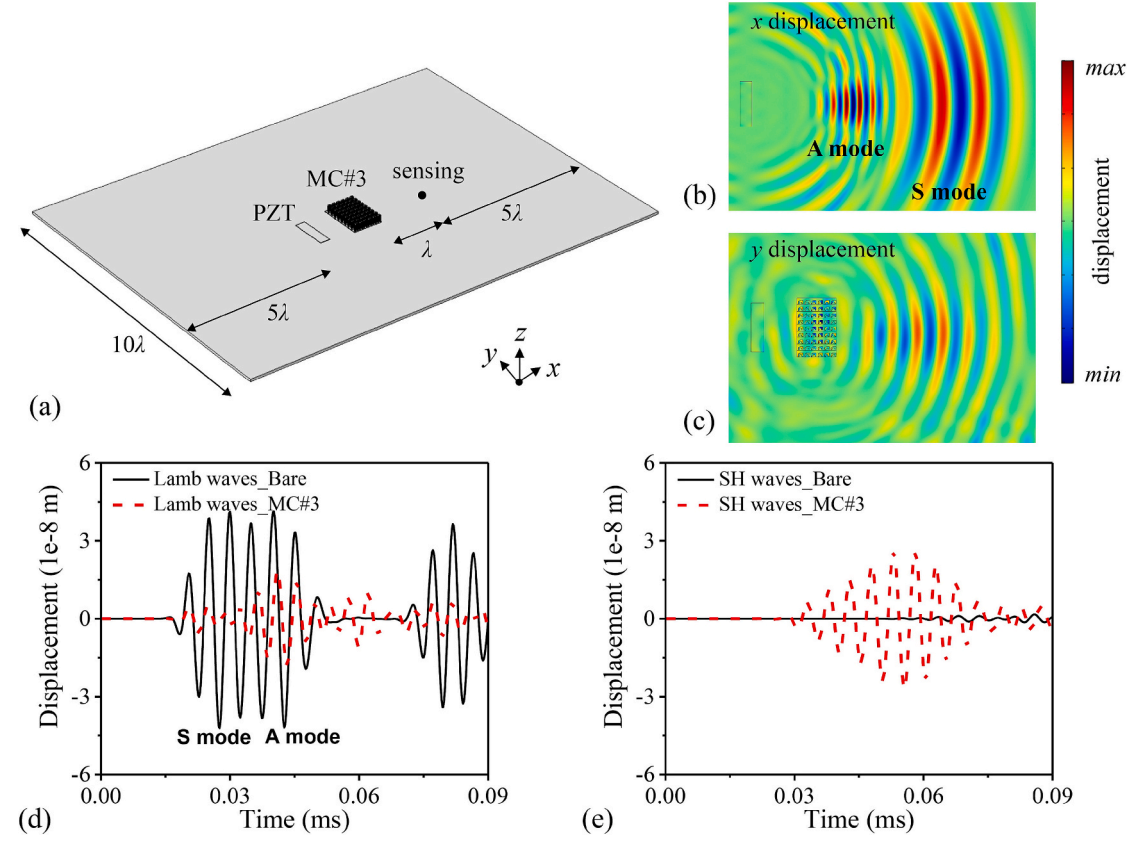


Fig. 12. (a) 3D full-field FE model (λ represents the wavelength of S mode Lamb wave at 200 kHz), displacement fields of (b) Lamb waves in the x direction in the bare plate and (c) SH waves in the y direction with the meta-converter, and time-domain signals of (d) Lamb waves and (e) SH waves.

4.2. Assessment of meta-converter performance

Step-by-step experiments, following the schematic diagram shown in Fig. 13(c), are carried out to assess the performance of the meta-converter. The bare plate (Case 1) is first tested to provide a reference for comparison. Then, meta-converter samples (Case 2) are surface-mounted to the plate to examine their mode-conversion capability through the measurement of SH waves. Fig. 14 presents the time-domain results with/without the meta-converter MC#3. It is observed that the deployment of the meta-converters results in a dramatic increase in the amplitudes of the measured SH waves, rising from 15 mV to 155 mV, thus confirming the capacity of the proposed designs. Meanwhile, strong SH waves are also shown to be generated at other excitation frequencies, such as 180, 190, 210 and 220 kHz (not all results are shown here). This phenomenon can be attributed to the feature of the designed meta-converter, which can operate effectively over a certain frequency band.

Furthermore, a gel test (Case 3), as shown in Fig. 15, is conducted to confirm the existence of SH waves, mainly for distinguishing them from Lamb waves [49,50]. In principle, the gel should cause the dissipation of Lamb waves, especially for the out-of-plane motions, but it does not visibly attenuate SH waves (in-plane motion). The comparison with/without the gel is presented in Fig. 16, with MC#3 installed. It can be seen that the added gel has no discernible impact on the signals. This provides additional evidence that the captured signals are indeed SH waves, and also corroborates the proposed meta-converter-based method for SH wave generation.

A d_{31} -type PZT-5H sensor (6 mm \times 6 mm \times 0.3 mm) (Case 4 and Case 5) is then used as the receiver to quantify the energy level of the Lamb waves excited by the PZT transducer, and to evaluate their changes due to the installation of the meta-converters. The PZT sensor is positioned 230 mm from the actuator. The time-domain signals in Fig. 17 show that the amplitude of the excited Lamb waves is around 1.8 V. After introducing the meta-converter MC#3, a reduction in the amplitude of the Lamb waves is observed, indicating that part of the Lamb wave energy has been converted into that of SH waves.

To further demonstrate the efficiency of the proposed method for SH wave generation, a conventional shear-type PZT transducer ($d_{15}=860~\mathrm{pm/V}$) (Case 6) with dimensions of 8 mm \times 8 mm \times 0.25 mm is employed as the actuator for comparison, which is placed 230 mm from the MsT sensor. Note there is a slight difference in the actuator-sensor distance between Case 2 and Case 6: 270 mm (PZT-MsT) and 230 mm (d_{15} PZT-MsT), respectively. When conducting experiment in Case 6, as shown in Fig. 13(c), the PZT actuator used in Case 2 is kept in place. The intention is to maintain the integrity of the experimental set-up as much as possible for subsequent

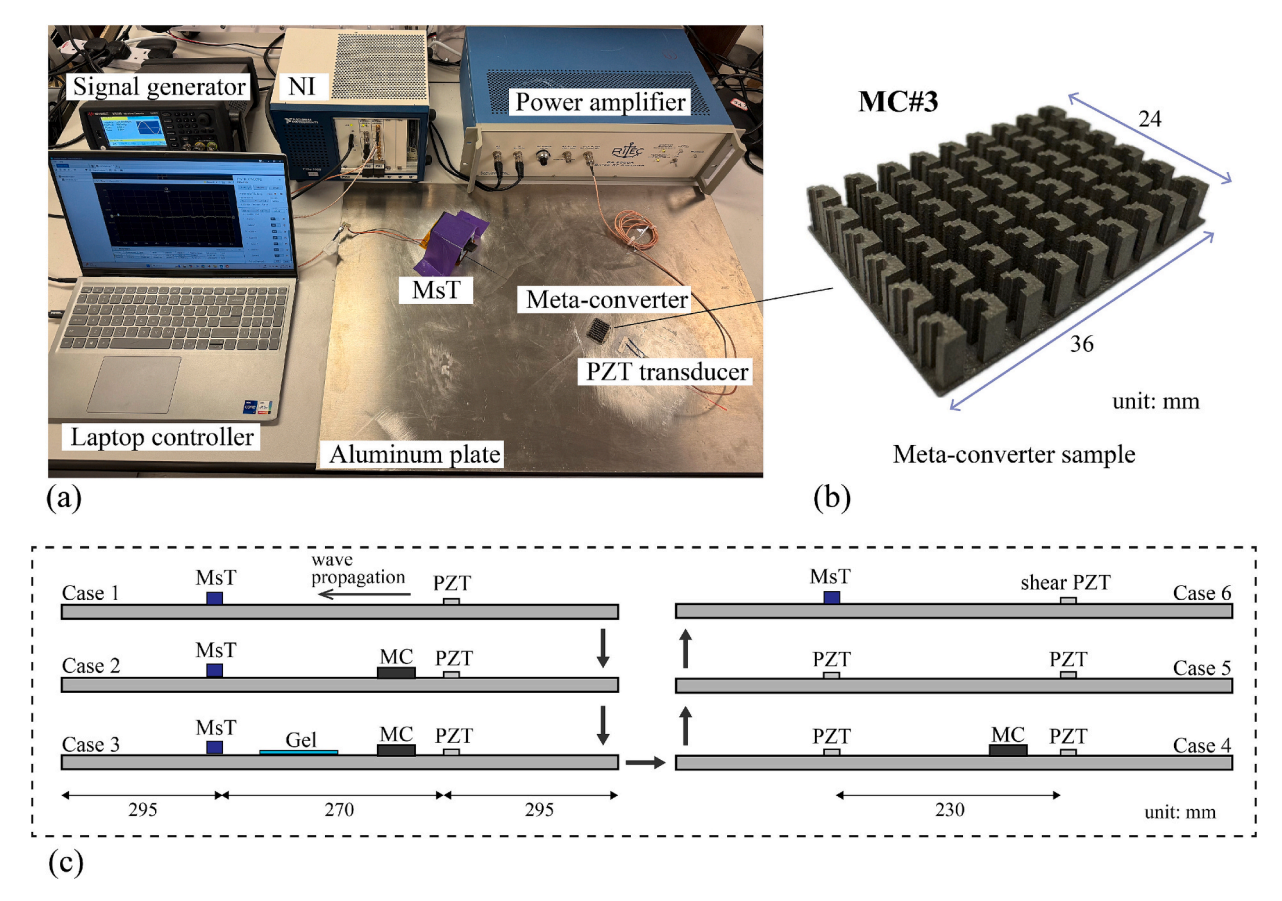


Fig. 13. (a) Experimental set-up, (b) the meta-converter sample MC#3, and (c) schematic of the step-by-step experimental procedure.

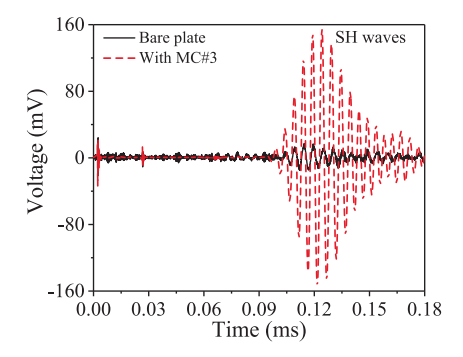
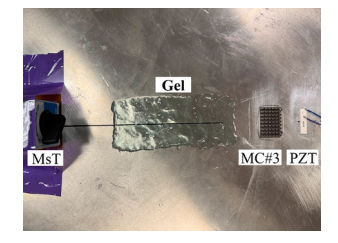


Fig. 14. Time-domain signals with/without the meta-converter sample MC#3.



 $\textbf{Fig. 15.} \ \ \text{Set-up of the gel test.}$

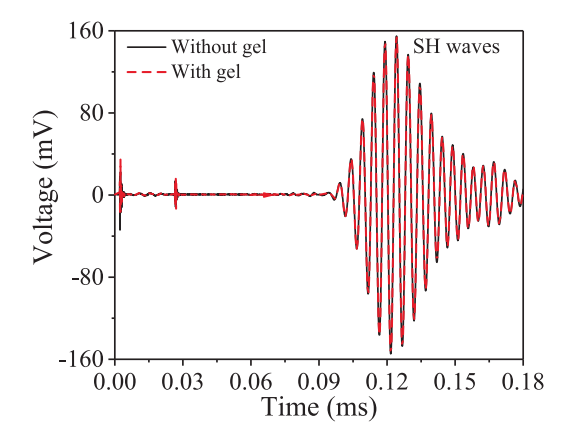


Fig. 16. Time-domain signals with/without using the gel, in the presence of the meta-converter MC#3.

analyses. Consequently, the shear-type PZT actuator in Case 6 is actually closer to the sensor, which should, in principle, produce stronger SH waves considering the effect of wave beam divergence. Despite that, the measured SH wave amplitude observed in Fig. 18 is significantly lower than that in Case 2 (in Fig. 14 using the proposed method), highlighting the higher efficiency of the proposed method for SH wave generation. Specifically, a wave packet around 0.06 ms is observed in Fig. 18, which corresponds to the second harmonic S0 mode Lamb waves induced by system nonlinearity [9,45]. Due to the close wavelength of the 200 kHz SH waves (15.6 mm) and 400 kHz S0 waves (13.4 mm), this secondary wave can be captured by the MsT, which, however, does not affect the extraction of the SH waves. Moreover, the present method compares favorably with other conventional transducers (e.g., d_{24} -type shear PZT transducers [21] and MsTs [8]) commonly employed in SHM for SH wave generation in terms of wave magnitudes. Thus, the effectiveness of the proposed method has been validated. Additionally, a different case at 150 kHz is also investigated, with the results presented in Appendix as supplementary evidence.

5. Conclusions

To tackle the difficulty in efficient excitation of SH waves, this study proposes a meta-converter design for SH wave generation through tactical mode conversion from Lamb waves excited by conventional PZT transducers. To achieve high-efficiency SH wave generation, topology optimization is conducted to tailor-make the add-on meta-converters on demand. The performance of the meta-converters is then systematically evaluated through both FE simulations and experimental validations.

In all tested cases, including Lamb waves of different modes and frequencies, the optimized meta-converters are shown to enable effective SH wave generation. Band structure analyses reveal that the hybrid modes caused by the meta-converters trigger strong coupling between Lamb waves and SH waves, resulting in efficient energy transfer between them. The efficacy of the designed meta-converter is demonstrated through time-domain response analyses. Wave fields and 2D-FFT analyses highlight the directional characteristics of the incident Lamb waves and the transmitted SH waves, respectively. Robustness analyses demonstrate the inherent property of the meta-converters for mode conversion, which is independent of the transducer size. Finally, experimental tests validate the effective enhancement of SH waves achieved by the designed meta-converters. Specifically, the amplitude of SH waves is increased significantly from 15 mV to 155 mV with the aid of the meta-converter, evidencing its efficacy for SH wave generation.

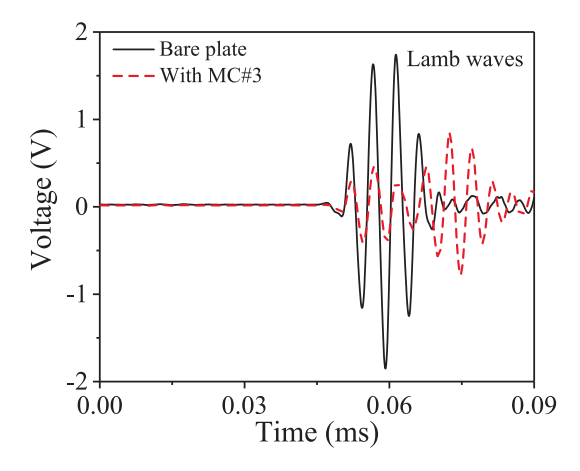


Fig. 17. Time-domain signals of Lamb waves with/without the meta-converter sample MC#3.

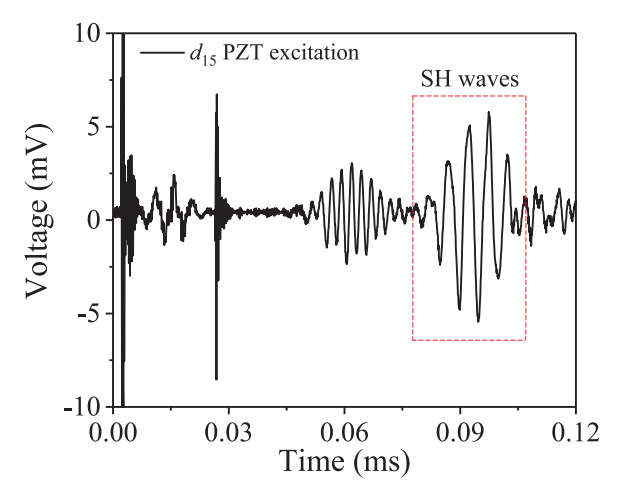


Fig. 18. Time-domain signals of SH waves excited by a d_{15} -type shear PZT transducer.

From an SHM perspective, the proposed method offers an alternative and more generic route for SH wave generation. It circumvents the installation inconvenience of EMATs in practical SHM implementations on one hand, and significantly elevates the energy level of the generated SH waves compared to traditional shear-type PZT transducers on the other hand. The proposed technique is expected to contribute to the development of SH-wave-based SHM technology. While this study demonstrating the feasibility of applying meta-converters for SH wave generation, further research is still warranted. For instance, a more in-depth understanding on the mode conversion mechanism would be necessary through developing a more comprehensive and systematic theoretical framework. This may involve characterizing the anisotropic properties of the meta-converters using a fully three-dimensional model.

CRediT authorship contribution statement

Ze Liu: Writing – review & editing, Writing – original draft, Validation, Methodology, Investigation, Formal analysis, Data curation, Conceptualization, Investigation, Methodology, Validation, Writing – original draft, Writing – review & editing. **Shengbo Shan:** Conceptualization, Formal analysis, Investigation, Supervision, Writing – review & editing. **Chuanzeng Zhang:** Resources, Supervision, Writing – review & editing. **Li Cheng:** Conceptualization, Funding acquisition, Project administration, Resources, Supervision, Writing – review & editing.

Funding

This work was supported by the Research Grants Council of Hong Kong Special Administrative Region (PolyU 152013/21E); the National Natural Science Foundations of China (12302114); the Natural Science Foundation of Shanghai (22ZR1462700); the Fundamental Research Funds for the Central Universities; and the Innovation and Technology Commission of the HKSAR Government to the Hong Kong Branch of National Rail Transit Electrification and Automation Engineering Technology Research Center (K-BBY1).

Declaration of competing interest

The authors declare that they have no known competing financial interests or personal relationships that could have appeared to influence the work reported in this paper.

Appendix A. Supplementary data

Supplementary data to this article can be found online at https://doi.org/10.1016/j.ymssp.2025.113516.

Data availability

Data will be made available on request.

References

[1] V. Giurgiutiu, Structural health monitoring: with piezoelectric wafer active sensors, Elsevier, 2007.

- [2] P. Li, S. Shan, F. Wen, L. Cheng, A fully-coupled dynamic model for the fundamental shear horizontal wave generation in a PZT activated SHM system, Mech. Syst. Sig. Process. 116 (2019) 916–932.
- [3] P. Rajagopal, M. Lowe, Short range scattering of the fundamental shear horizontal guided wave mode normally incident at a through-thickness crack in an isotropic plate, J. Acoust. Soc. Am. 122 (2007) 1527–1538.
- [4] F. Wen, S. Shan, R. Radecki, W.J. Staszewski, L. Cheng, Shear-lag modelling of surface-bonded magnetostrictive transducers for shear horizontal wave generation in a non-ferromagnetic plate, Smart Mater. Struct. 30 (2021) 035026.
- [5] C.J. Lissenden, Nonlinear ultrasonic guided waves—Principles for nondestructive evaluation, J. Appl. Phys. 129 (2021) 021101.
- [6] H. Miao, Q. Zhu, Y. Zhang, Q. Kan, P. Wang, W. Zhang, G. Kang, SH guided wave excitation in rails for defect and stress monitoring, Mech. Syst. Sig. Process. 224 (2025) 112064.
- [7] Y. Liu, V.K. Chillara, C.J. Lissenden, On selection of primary modes for generation of strong internally resonant second harmonics in plate, J. Sound Vib. 332 (2013) 4517–4528.
- [8] F. Wen, S. Shan, L. Cheng, Third harmonic shear horizontal waves for material degradation monitoring, Struct. Health Monit. 20 (2021) 475-483.
- [9] F. Wen, S. Shan, L. Cheng, Immunity of the second harmonic shear horizontal waves to adhesive nonlinearity for breathing crack detection, Struct. Health Monit. 21 (2022) 2340–2353.
- [10] C. Vasile, R. Thompson, Excitation of horizontally polarized shear elastic waves by electromagnetic transducers with periodic permanent magnets, J. Appl. Phys. 50 (1979) 2583–2588.
- [11] H. Kwun, K. Bartels, Magnetostrictive sensor technology and its applications, Ultrasonics 36 (1998) 171-178.
- [12] S. Shan, M. Hasanian, H. Cho, C.J. Lissenden, L. Cheng, New nonlinear ultrasonic method for material characterization: Codirectional shear horizontal guided wave mixing in plate, Ultrasonics 96 (2019) 64–74.
- [13] R.B. Thompson, A model for the electromagnetic generation and detection of Rayleigh and Lamb waves, IEEE Trans. Sonics Ultrason. 20 (1973) 340-346.
- [14] R. Ribichini, F. Cegla, P.B. Nagy, P. Cawley, Study and comparison of different EMAT configurations for SH wave inspection, IEEE Trans. Ultrason. Ferroelectr. Freq. Control 58 (2012) 2571–2581.
- [15] S. Hill, S. Dixon, Frequency dependent directivity of periodic permanent magnet electromagnetic acoustic transducers, NDT E Int. 62 (2014) 137–143.
- [16] H.M. Seung, C.I. Park, Y.Y. Kim, An omnidirectional shear-horizontal guided wave EMAT for a metallic plate, Ultrasonics 69 (2016) 58-66.
- [17] Y. Du, J. Cai, Q. Kan, Q. Zhang, P. Wang, H. Miao, G. Kang, Time-delayed layer-based piezoelectric transducer for unidirectional excitation and reception of SH guided wave, Mech. Syst. Sig. Process. 193 (2023) 110268.
- [18] P. Belanger, G. Boivin, Development of a low frequency omnidirectional piezoelectric shear horizontal wave transducer, Smart Mater. Struct. 25 (2016) 045024.
- [19] W. Zhou, H. Li, F.-G. Yuan, Fundamental understanding of wave generation and reception using d36 type piezoelectric transducers, Ultrasonics 57 (2015) 135–143.
- [20] H. Miao, S. Dong, F. Li, Excitation of fundamental shear horizontal wave by using face-shear (d36) piezoelectric ceramics, J. Appl. Phys. 119 (2016) 174101.
- [21] H. Miao, Q. Huan, Q. Wang, F. Li, A new omnidirectional shear horizontal wave transducer using face-shear (d24) piezoelectric ring array, Ultrasonics 74 (2017) 167–173.
- [22] H. Miao, Q. Huan, F. Li, Excitation and reception of pure shear horizontal waves by using face-shear d24 mode piezoelectric wafers, Smart Mater. Struct. 25 (2016) 11LT01.
- [23] H. Qiu, M. Chen, F. Li, Selective excitation of high-order shear horizontal wave (SH1) by using a piezoelectric interdigital transducer, Mech. Syst. Sig. Process. 165 (2022) 108390.
- [24] Z. Liu, X. Zhang, Y. Mao, Y. Zhu, Z. Yang, C.T. Chan, P. Sheng, Locally resonant sonic materials, Science 289 (2000) 1734–1736.
- [25] A.-L. Chen, Y.-S. Wang, Y.-F. Wang, H.-T. Zhou, S.-M. Yuan, Design of acoustic/elastic phase gradient metasurfaces: principles, functional elements, tunability, and coding, Appl. Mech. Rev. 74 (2022) 020801.
- [26] X. Yang, Y.Y. Kim, Topology optimization for the design of perfect mode-converting anisotropic elastic metamaterials, Compos. Struct. 201 (2018) 161–177.
- [27] Z. Liu, S. Shan, L. Cheng, Meta-structure enhanced second harmonic SO waves for material microstructural changes monitoring, Ultrasonics 139 (2024) 107295.
- [28] M. Farhat, S. Guenneau, S. Enoch, Ultrabroadband elastic cloaking in thin plates, Phys. Rev. Lett. 103 (2009) 024301.
- [29] Z. Zhou, S. Huang, D. Li, J. Zhu, Y. Li, Broadband impedance modulation via non-local acoustic metamaterials, Natl. Sci. Rev. 9 (2022) nwab171.
- [30] Y. Tian, Y. Shen, X. Qin, Z. Yu, Enabling the complete mode conversion of Lamb waves into shear horizontal waves via a resonance-based elastic metamaterial, Appl. Phys. Lett. 118 (2021) 014101.
- [31] J.M. Kweun, H.J. Lee, J.H. Oh, H.M. Seung, Y.Y. Kim, Transmodal Fabry-Pérot resonance: theory and realization with elastic metamaterials, Phys. Rev. Lett. 118 (2017) 205901.
- [32] Y. Tian, Y. Song, Y. Shen, Z. Yu, A metamaterial ultrasound mode convertor for complete transformation of Lamb waves into shear horizontal waves, Ultrasonics 119 (2022) 106627.
- [33] O. Sigmund, J. Søndergaard Jensen, Systematic design of phononic band–gap materials and structures by topology optimization, Philos. Trans. r. Soc. Lond. A Math. Phys. Eng. Sci. 361 (2003) 1001–1019.
- [34] H.-W. Dong, C. Shen, Z. Liu, S.-D. Zhao, Z. Ren, C.-X. Liu, X. He, S.A. Cummer, Y.-S. Wang, D. Fang, Inverse design of phononic meta-structured materials, Mater. Today (2024).
- [35] Z. Liu, H.-W. Dong, G.-L. Yu, Topology optimization of periodic barriers for surface waves, Struct. Multidiscip. Optim. 63 (2021) 463–478.
- [36] Z. Liu, S.-B. Shan, H.-W. Dong, L. Cheng, Topologically customized and surface-mounted meta-devices for Lamb wave manipulation, Smart Mater. Struct. 31 (2022) 065001.
- [37] V. Giurgiutiu, Tuned Lamb wave excitation and detection with piezoelectric wafer active sensors for structural health monitoring, J. Intell. Mater. Syst. Struct. 16 (2005) 291–305.
- [38] Z. Su, C. Zhou, M. Hong, L. Cheng, Q. Wang, X. Qing, Acousto-ultrasonics-based fatigue damage characterization: Linear versus nonlinear signal features, Mech. Syst. Sig. Process. 45 (2014) 225–239.
- [39] J.H. Holland, Adaptation in natural and artificial systems: an introductory analysis with applications to biology, control, and artificial intelligence, MIT Press (1992).
- [40] J. Rong, W. Ye, S. Zhang, Y. Liu, Frequency-coded passive multifunctional elastic metasurfaces, Adv. Funct. Mater. 30 (2020) 2005285.
- [41] H.-W. Dong, C. Shen, S.-D. Zhao, W. Qiu, H. Zheng, C. Zhang, S.A. Cummer, Y.-S. Wang, D. Fang, L. Cheng, Achromatic metasurfaces by dispersion customization for ultra-broadband acoustic beam engineering, Natl. Sci. Rev. 9 (2022) nwac030.
- [42] Z. Liu, H.-W. Dong, G.-L. Yu, L. Cheng, Achieving ultra-broadband and ultra-low-frequency surface wave bandgaps in seismic metamaterials through topology optimization, Compos. Struct. 295 (2022) 115863.
- [43] H.-W. Dong, X.-X. Su, Y.-S. Wang, C. Zhang, Topological optimization of two-dimensional phononic crystals based on the finite element method and genetic algorithm, Struct. Multidiscip. Optim. 50 (2014) 593–604.
- [44] Z. Liu, S. Shan, L. Cheng, A0 mode lamb wave propagation in a nonlinear medium and enhancement by topologically designed metasurfaces for material degradation monitoring, Nonlinear Dyn. 112 (2024) 16963–16981.
- [45] S. Shan, L. Cheng, P. Li, Adhesive nonlinearity in Lamb-wave-based structural health monitoring systems, Smart Mater. Struct. 26 (2016) 025019.
- [46] J.M. De Ponti, L. Jorio, E. Riva, R. Ardito, F. Braghin, A. Corigliano, Selective mode conversion and rainbow trapping via graded elastic waveguides, Phys. Rev. Appl 16 (2021) 034028.
- [47] J. Achenbach, Wave propagation in elastic solids, Elsevier, 2012.

- [48] M.M. Sigalas, Elastic and acoustic wave band structure, J. Sound Vib. 158 (1992) 377–382.[49] S. Shan, L. Cheng, Mixed third harmonic shear horizontal wave generation: interaction between primary shear horizontal wave and second harmonic Lamb
- wave, Smart Mater. Struct. 28 (2019) 085042.

 [50] M. Hasanian, C.J. Lissenden, Second order harmonic guided wave mutual interactions in plate: Vector analysis, numerical simulation, and experimental results, J. Appl. Phys. 122 (2017) 084901.